

Modeling and simulation of coagulation according to DLVO-theory in a continuum model for electrolyte solutions

Matthias Herz¹ and Peter Knabner¹

¹*Department of Mathematics, University of Erlangen-Nürnberg, Cauerstr. 11, D-91058 Erlangen, Germany
Fax: +49 +9131 85-67225; Tel: +49 +9131 85-67238; E-mail: matthias.herz@fau.de*

May 27, 2016

Abstract

This paper presents a model of coagulation in electrolyte solutions. In this paper, the coagulation process is modeled according to DLVO-theory, which is an atomistic theory. On the other hand, we describe the dynamics in the electrolyte solutions by the Poisson–Nernst–Planck system, which is a continuum model. The contribution of this paper is to include the atomistic description of coagulation based on DLVO-theory in the continuum Poisson–Nernst–Planck system. Thereby, we involve information from different spatial scales. For this reason, the presented model accounts for the short-range interactions and the long-range interactions, which drive the coagulation process. Furthermore, many-body effects are naturally included as the resulting model is a continuum model.

Keywords: Coagulation, aggregation, DLVO-theory, electrolyte solution, Poisson–Nernst–Planck system, electrohydrodynamics.

1 Introduction

In multicomponent solutions, an ubiquitous process is the formation of particle clusters, which is commonly referred to as coagulation. Particle clusters arise when particles of the same chemical species collide and afterwards stick together due to attractive particle interactions. The prototypical example of attractive particle interactions are ever present van der Waals interactions. These attractive interactions originate from electromagnetic fluctuations, cf. [6, 10, 30, 40, 43, 51, 56]. Moreover, van der Waals interactions are short-range interactions, which are active over a few nanometers. Thus, van der Waals interactions are solely relevant for particles close to contact. On the other hand, for particles far from contact the driving force behind collisions is thermal motion and for charged particles additionally electric drift motion along the field lines of a long-range electric field. However, in particular for electrically charged particles there is an additional short-range electric repulsion between equally charged particles, which counteracts attractive van der Waals interactions. Thus, in electrolyte solutions coagulation is caused by the interplay of long-range thermal motion, long-range electric fields, short-range attractive van der Waals interactions, and short-range electric repulsion of charged particles of the same chemical species. More precisely, van der Waals interactions, moderate thermal motion, and moderate electric drift motion trigger the coagulation process, whereas strong thermal motion, strong electric drift motion, and electrostatic repulsion prevent the particles from coagulation.

Furthermore, coagulation is the central process, which determines the stability properties of electrolyte solutions. Here, an electrolyte solution is stable, if dissolved particles remain dissolved, whereas an electrolyte solution is unstable, if dissolved particles form clusters, i.e., if the particles coagulate.

Classically, coagulation in electrolyte solutions is explained by the so-called DLVO-theory, which is at the heart of colloid science and electrochemistry, cf. [15, 23, 25, 34, 35, 37, 41, 46]. This short-range theory describes the interplay of short-range attractive van der Waals forces and short-range electrostatic repulsion in terms of a pair potential. Here, “pair potential” refers to an energy

potential, that describes for two particles the energy of interaction as function of distance. This means, that DLVO-theory explicitly resolves single particles and thus, is an atomistic theory. However, DLVO-theory solely captures the energetic picture of coagulation, i.e., whether coagulation is an energetic favorable process or not. Hence, informations about coagulation kinetics are absent in DLVO-theory. Regarding the dynamics of coagulation, classical models are the Smoluchowski coagulation equation or, more generally, population balance equations, cf. [1, 2, 7, 8, 12, 21, 23, 24, 26, 29, 32, 33, 37, 39, 44, 48, 52, 54]. Thus, a comprehensive model of coagulation has to include both, the energetic picture, and the kinetic picture.

In this paper, we describe the interplay of long-range thermal motion (=diffusion) and long-range electric drift motion (=electro diffusion) by means of the Navier–Stokes–Poisson–Nernst–Planck system. This system is a thermodynamically consistent and classical continuum model for electrolyte solutions. However, as the characteristic feature of continuum models is to simultaneously track a large number of particles by means of particle concentrations, these models do not resolve single particles and thus, continuum models have no access to atomistic DLVO-theory. This is a serious restriction, as coagulation of particles occurs through the interplay of long-range interactions governed by the Navier–Stokes–Poisson–Nernst–Planck system and short-range interactions governed by DLVO-theory. In this paper, we derive a model for coagulation in electrolyte solutions, which fully captures the process of coagulation in the sense that we successfully combine the continuum Navier–Stokes–Poisson–Nernst–Planck system with the atomistic DLVO-theory. Thereby, we obtain a micro-macro model, which naturally accounts for the short-range picture, the long-range picture, the energetic picture, and the kinetic picture.

The rest of this paper is organized as follows: Firstly, we present the governing equations in Section 2. Next, in Section 3, we propose an ansatz for coagulation kinetics, and we show how to include DLVO-theory in a continuum model. Finally, in Section 4, we present the resulting model and some numerical simulations.

2 The general governing Equations

We adopt the Navier–Stokes–Poisson–Nernst–Planck system as the governing equations for the considered electrolyte solutions. Note, that this system is thermodynamically consistent (especially the thermodynamical consistency of this system, we investigate in a forthcoming paper) model for isothermal, incompressible electrolyte solutions with an electrically neutral solvent. More precisely, this system consists of the following set of equations.

1. Poisson’s equation: We have for the electric field $\mathbf{E} = -\nabla\Phi$, and Φ solves

$$-\nabla \cdot (\epsilon_r \nabla \Phi) = \frac{1}{\epsilon_0} \rho_f \quad \text{with} \quad \rho_f = \sum_l \frac{e_0 z_l}{m_l} \rho_l. \quad (2.1a)$$

Here, ϵ_0 is the electric permittivity, ϵ_r the relative permittivity of the medium, ρ_f is the free charge density, e_0 the elementary charge. For $l \in \{1, \dots, L\}$, ρ_l is the mass density of the l th solute, m_l the molecular mass of the l th solute, and z_l the valency of the l th solute. Furthermore, we have indexed the chemical species such the the solvent is the L th chemical species. As we assume an electrically neutral solvent, we have $z_L = 0$.

2. Nernst–Planck equations: For $l \in \{1, \dots, L-1\}$, we have

$$\partial_t \rho_l + \nabla \cdot \left(\rho_l \mathbf{u} - d_l \nabla \rho_l - \frac{e_0 d_l z_l}{k_b T} \rho_l \mathbf{E} \right) = r_l, \quad (2.1b)$$

Here, d_l is the diffusion coefficient of the l th solute, k_b the Boltzmann constant, and T the constant temperature. Furthermore, the ansatzes for the mass production rates r_l are given by mass action kinetics, cf. [3, 14, 45, 53, 55]. Note, that we deal with incompressible mixtures. This is modeled

by a constant total density $\rho := \sum_l \rho_l \equiv \text{const}$, which leads to the following incompressibility constraint (2.1c). cf. [11, 36, 42]. Thus, we obtain the solvent concentration ρ_L by $\rho_L = \rho - \sum_l^{L-1} \rho_l$, cf. [11, 45].

3. Navier–Stokes equations: For the barycentric momentum density $\rho \mathbf{u}$ holds

$$\nabla \cdot \mathbf{u} = 0, \quad (2.1c)$$

$$\rho \partial_t \mathbf{u} + \rho \nabla \cdot (\mathbf{u} \otimes \mathbf{u}) = -\nabla p + 2\eta \Delta \mathbf{u} + \rho_f \mathbf{E}. \quad (2.1d)$$

Here, \mathbf{u} is the barycentric velocity field and p the pressure of the mixture.

To introduce the new coagulation model within the framework of Navier–Stokes–Poisson–Nernst–Planck systems, we subsequently reduce the preceding equations (2.1a)–(2.1d) to a setting, which allows to concentrate on coagulation effects. More precisely, we henceforth confine ourselves to the following setting:

- (M1) We consider electrolyte solutions with four components, i.e, we have $L = 4$.
- (M2) We suppose, the four components are given by the neutral solvent $\rho_s := \rho_4$, a positively charged chemical species $\rho^+ := \rho_1$, and a negatively charged chemical species $\rho^- := \rho_2$. Furthermore, we assume that solely the positively charged chemical species can coagulate and form aggregates. To resolve these aggregates, we introduce an additional chemical species $\rho_a^+ := \rho_3$.
- (M3) Henceforth, we label the quantities for ρ^+ by the superscript $+$, the quantities for ρ^- by $-$, the quantities for ρ_a^+ by $^+$, and the quantities for ρ_s by the subscript s .
- (M4) We assume, the aggregates are subject to gravitational forces. Hence, we have with the gravitational acceleration field \mathbf{g} [m/s^2] the additional term $\frac{d_3 m_3}{k_b T} \rho_a^+ \mathbf{g}$ [$kg/(m^2 s)$] in the mass flux for ρ_a^+ .
- (M5) We suppose symmetric charges $z^+ = z = -z^-$, and $r_- = 0$.
- (M6) We assume, that the single reactive mechanism within the mixture is the coagulation of the positively charged chemical species, which can be described by a reaction rate R^{coag} . Hence, the mass production rate r^+ reads as $r^+ = m^+ s^+ R^{coag}$. Similarly the mass production rate r_a^+ is given by $r_a^+ = m_a^+ s_a^+ R^{coag}$, cf. [4, 11, 45]

Thus, for the rest of this paper the governing equations are given by

1. Poisson's equation: We have for the electric field $\mathbf{E} = -\nabla \Phi$, and Φ solves

$$-\nabla \cdot (\epsilon_r \nabla \Phi) = \frac{1}{\epsilon_0} \rho_f \quad \text{with} \quad \rho_f = \sum_l \frac{e_0 z_l}{m_l} \rho_l = \frac{z \rho^+}{m^+} - \frac{z \rho^-}{m^-} + \frac{z_a^+ \rho_a^+}{m_a^+}. \quad (2.2a)$$

2. Nernst–Planck equations: We have

$$\partial_t \rho^+ + \nabla \cdot \left(\rho^+ \mathbf{u} - d^+ \nabla \rho^+ - \frac{e_0 d^+ z}{k_b T} \rho^+ \mathbf{E} \right) = m^+ s^+ R^{coag}, \quad (2.2b)$$

$$\partial_t \rho^- + \nabla \cdot \left(\rho^- \mathbf{u} - d^- \nabla \rho^- + \frac{e_0 d^- z}{k_b T} \rho^- \mathbf{E} \right) = 0, \quad (2.2c)$$

$$\partial_t \rho_a^+ + \nabla \cdot \left(\rho_a^+ \mathbf{u} - d_a^+ \nabla \rho_a^+ - \frac{e_0 d_a^+ z_a^+}{k_b T} \rho_a^+ \mathbf{E} + \frac{d_a^+ m_a^+}{k_b T} \rho_a^+ \mathbf{g} \right) = m_a^+ s_a^+ R^{coag}. \quad (2.2d)$$

Here, the solvent concentration ρ_s is obtained by $\rho_s = \rho - \rho^+ - \rho^- - \rho_a^+$.

3. Navier–Stokes equations: For the barycentric momentum density holds

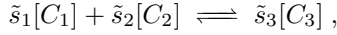
$$\nabla \cdot \mathbf{u} = 0, \quad (2.2e)$$

$$\rho \partial_t \mathbf{u} + \rho \nabla \cdot (\mathbf{u} \otimes \mathbf{u}) = -\nabla p + 2\eta \Delta \mathbf{u} + \rho_f \mathbf{E}. \quad (2.2f)$$

In the next section, we derive a new ansatz for the rate function R^{coag} , which models the process of coagulation.

3 Coagulation Kinetics including DLVO-theory

First of all, we note that the reaction rates in equations (2.2b)–(2.2d) are reaction rates according to mass action law, cf. [3, 14, 45, 53, 55]. More precisely, from these references we recall that provided the stoichiometry of a chemical reaction reads as



the corresponding reaction rate function R is given with the mass fractions y_l and the stoichiometric coefficients $s_1 := -\tilde{s}_1$, $s_2 := -\tilde{s}_2$, $s_3 := \tilde{s}_3$ by

$$R = R^f - R^b = k^f y_1^{-s_1} y_2^{-s_2} - k^b y_3^{s_3}. \quad (3.1)$$

According to this equation the forward reaction takes place, if both reactants are present. Hence, the above stoichiometry implicitly contains the assumption that the single barrier, which hinders the reactions is the presence of the reactants. However, in some situations other barriers such as certain energy barriers truly exist. Provided we formulate such a barrier with a function g as an inequality constraint $g > 0$, the stoichiometry now is given by



Here, the condition $g > 0$ above the arrows indicates that the reaction solely takes place if we have $g > 0$. Thus, besides the presence of the reactants the reaction rate is triggered by a barrier function $H(g)$, which is given with the Heaviside function H by

$$(t, x) \mapsto H(g(t, x)) = \begin{cases} 1, & \text{if } g(t, x) > 0, \\ 0, & \text{if } g(t, x) \leq 0. \end{cases}$$

Thus, the rate functions R for reactions, which include inequality constraints, are given by

$$R = \underbrace{H(g)}_{\text{barrier function}} \underbrace{R^{kin}}_{\text{reaction kinetics}} = \begin{cases} R^{kin}, & \text{if } g > 0, \\ 0, & \text{if } g \leq 0. \end{cases} \quad (3.3)$$

Here, the barrier function $H(g)$ triggers the reaction according to the given inequality constraint and R^{kin} describes the reaction kinetics. Thus, the mass action law rate function R corresponding to (3.2) is given with (3.1) and (3.3) by

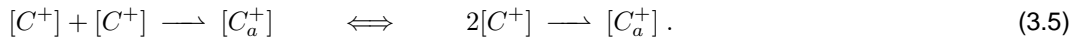
$$R = H(g) (k^f y_1^{-s_1} y_2^{-s_2} - k^b y_3^{s_3}) = \begin{cases} k^f y_1^{-s_1} y_2^{-s_2} - k^b y_3^{s_3}, & \text{if } g > 0, \\ 0, & \text{if } g \leq 0. \end{cases}$$

Note, that reaction rate functions including the Heaviside function have previously been introduced in a different context in [28]. Subsequently, we introduce the coagulation rate R^{coag} exactly as reaction rate of the above type. More precisely, to include in the coagulation rate R^{coag} the energetic picture according to DLVO-theory as well as the kinetic picture of coagulation, we assume for R^{coag} the ansatz

$$R^{coag} = H(g^{DLVO}) R^{coag,kin}. \quad (3.4)$$

Here, g^{DLVO} has to capture the energy barrier according to DLVO-theory and $R^{coag,kin}$ the coagulation kinetics. In the rest of this section, we firstly derive a formula for $R^{coag,kin}$, and secondly a formula for g^{DLVO} .

In this passage, we introduce the coagulation kinetics. For that purpose, we assume that the aggregates $[C_a^+]$ are made of doublets of dissolved particles $[C^+]$. This leads us to the stoichiometry



As this stoichiometry is a crucial part of the proposed model, we now clarify this ansatz.

- (i) The arrow “ \rightarrow ” indicates that we consider coagulation as an irreversible reaction. This comes from the fact that we suppose the aggregates to be solid aggregates. For solids the dissolution rate just depends on the intensity of the thermal motion of the particles within the solid structure, i.e., the dissolution rate is a function of temperature, cf. [3, 14]. As we consider isothermal electrolyte solutions, the dissolution rate is constant. Henceforth, we assume this constant to be zero.
- (ii) The assumption that the aggregates are made of doublets leads to a quadratic reaction rate. This corresponds to the Smoluchowski coagulation equation, which is based on quadratic coagulation kernels, cf. [12, 23, 37].
- (iii) Note, that the aggregates $[C_a^+]$ are of the same chemical species as $[C^+]$. Furthermore, in (M4) we supposed that the aggregates are subject to gravity. In the framework of population balance equations this means, we have separated the positively charged particles into two size classes. The first size class contains the particles $[C^+]$, which are sufficiently small such that gravitational effects can be neglected, and such that we can consider this particles to be dissolved. The second size class contains the aggregates $[C_a^+]$, which are sufficiently large such that they are subject to gravity, and such that we can consider the particles of this size class to be solid aggregates.
- (iv) The preceding interpretation of the model in terms of size classes reveals that only a fraction of doublets $2[C^+]$ leads to an aggregate $[C_a^+]$ in the second size class. More precisely, the particles $[C^+]$ can form doublets, doublets of doublets, etc. Only after repeatedly forming doublets of doublets, the resulting aggregates have grown large enough to belong to the second size class $[C_a^+]$. Hence, the stoichiometry (3.5) includes a certain latency due to repeatedly formation of doubles. Thus, the forward reaction rate constant k^f must account for this latency factor.
- (v) From (3.5), we know that the stoichiometric coefficients are given by $s^+ = -2$, $s_a^+ = 1$, cf. [3, 14, 53, 55]. Thus, we define the valencies by $z_a^+ = 2z^+$, and the molecular masses by $m_a^+ = 2m^+$. This choices ensure the conservation of mass, i.e., $m^+ s^+ R^{coag} + m_a^+ s_a^+ R^{coag} = 0$, and the conservation of charges, i.e., $e_0 z^+ s^+ R^{coag} + e_0 z_a^+ s_a^+ R^{coag} = 0$, cf. [4, 11, 45].

Altogether, we deduce from (3.5) that the coagulation kinetics are given by

$$R^{coag,kin} = k^f (y^+)^2. \quad (3.6)$$

As to the energy barrier according to DLVO-theory, we first recall that DLVO-theory describes the interplay between short-range electrostatic repulsion and short-range attractive van der Waals interactions, cf. [23, 34, 37]. Van der Waals interactions originate from electromagnetic fluctuations, cf. [6, 10, 30, 40, 43, 51, 56], and thus, the short range of van der Waals interactions inherently lies in the nature of van der Waals interactions. Opposed to this, electrostatic interactions are commonly considered to be long-range interactions. However, in electrolyte solutions the charge of a single particle is screened over a very short distance by oppositely charged particles. Consequently, owing to this screening, the charge of a particle is active only in a very small neighborhood, which is commonly referred to as the electric double layer (EDL), cf. [23, 25, 37, 46, 51]. Hence, the electrostatic repulsion between equally charged particles takes place as short-range interaction between their EDLs. More precisely, two equally charged particles only electrically interact provided their EDLs overlap. As a typical thickness of a EDL is 10 nm, cf. [23, 37], particles have to approach very close for overlapping EDLs. This screening of electrostatic interactions to short-range EDL interactions in electrolyte solutions is the deeper reason why van der Waals interactions become active in the first place.

Following the well-known derivations in [23, 25, 34, 37, 46, 51], DLVO-theory can be condensed by means of the so-called DLVO-potential V^{tot} , which is given by

$$V^{tot} = V^{el} + V^{vdw}.$$

Here, V^{el} is the potential accounting for electrostatic repulsion, and V^{vdw} the potential accounting for van der Waals interactions. More precisely, V^{el} describes the electrostatic repulsion between two infinite plates separated at distance d and V^{vdw} describes nonretarded van der Waals interactions

between two infinite plates separated at distance d . These potentials are given according to [23, Chapter 12.6] by

$$V^{el}(d) = \frac{64n_b k_b T}{\kappa} \exp(-\kappa d) \quad \text{and} \quad V^{vdw}(d) = -\frac{A}{12\pi d^2}.$$

Here, κ^{-1} [m] is the Debye length, n_b the number bulk concentration of the negatively charged counterions, and A [J] the Hamaker constant. These formulas show, that the DLVO-potential $V^{tot} = V^{tot}(d)$ is a pair potential, which expresses the interaction energy between two particles as function of interparticle distance d .

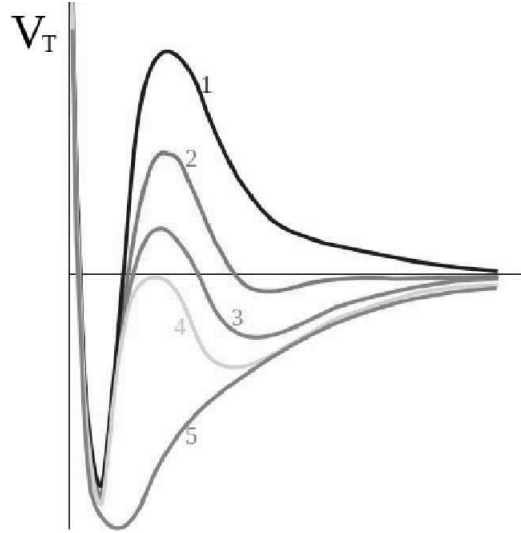


Figure 1: Ideal-typical plots of the DLVO-potential, cf. [13]

Furthermore, we have $V^{tot} < 0$ in case of attractive interaction energies and $V^{tot} > 0$ in case of repulsive interaction energies. Figure 1 depicts some ideal-typical plots of the DLVO-potential. This figure reveals two characteristic features of the DLVO-potential. Firstly, the DLVO-potential possesses an absolute minimum, which is the so-called primary minimum, cf. [23, 25, 37, 46, 51]. The DLVO-potential V^{tot} reaches this primary minimum precisely in case of coagulation. Hence, from an energy minimizing perspective, coagulation is the energetically favorable state. However, the second characteristic feature of the DLVO-potential V^{tot} is the energy barrier, which is depicted by the local maximum in the respective curves in Figure 1. This local maximum of the DLVO-potential is exactly the condensed description of the energy barrier due to electrostatic repulsion, which prevents the particles from coagulation. In curve 5 this energy barrier is absent, as this curve solely depicts the attractive part V^{vdw} . However, the essential observation from Figure 1 is that the local maximum only leads to an energy barrier, if the value of the DLVO-potential V^{tot} at this point is positive, as positive values mean repulsion. Consequently, provided the DLVO-potential V^{tot} is given by curve 4, we have no energy barrier. Moreover, as V^{tot} has only nonpositive values along curve 4, this curve depicts a purely nonrepulsive potential V^{tot} . Thus, in this situation coagulation can unconditionally take place. Consequently, the succinct criterion for such a nonrepulsive situation is a double zero of V^{tot} , i.e.,

$$V^{tot} = 0 = (V^{tot})'.$$

Following the calculations in [23], we firstly solve for $(V^{tot})' = 0$. Thereby, we obtain with the Debye-length κ^{-1} the critical point $x_* = 2/\kappa$. Note, that in [23] the Debye-length κ^{-1} is defined by

$$\kappa := \left(\frac{e_0^2 z^2 n_b}{\epsilon_r \epsilon_0 k_b T} \right)^{\frac{1}{2}}.$$

Substituting $x_* = 2/\kappa$ and the preceding definition of κ into $V^{tot}(x_*) = 0$, yields together with $z^2 = (z^-)^2$ an equation, which can be solved for the number bulk concentration n_b . Running through the calculations in [23] shows that this leads finally for the mass bulk concentration ρ_b of the negatively charged particles to¹

$$\rho_b := m^- n_b = 1000m^- \frac{(4\pi\epsilon_0)^3 0.107\epsilon_r^3 (k_b T)^5}{A^2 (e_0 z^-)^6} =: c.c.c.$$

The value of the right hand side is a given constant, which depends on several parameters. This constant is commonly referred to as the critical coagulation concentration (*c.c.c.*). Hence, the succinct criterion for an energy barrier is

$$\begin{aligned} \rho_b < c.c.c. &\implies V^{tot} > 0 \text{ at the local maximum} &\implies &\text{energy barrier,} \\ \rho_b \geq c.c.c. &\implies V^{tot} \leq 0 \text{ at the local maximum} &\implies &\text{no energy barrier.} \end{aligned} \quad (3.7)$$

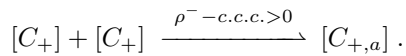
Here, it is essential that the inequality $\rho_b \stackrel{\geq}{\leq} c.c.c.$ involves a macroscopic quantity ρ_b on the left-hand side and a microscopic quantity *c.c.c.* on the right-hand side. More precisely, we already mentioned that DLVO-theory captures the interplay of van der Waals attraction and electrostatic repulsion of two particles with overlapping EDLs. Thus, DLVO-theory draws a detailed microscopic picture on spatial scales, which are not resolved in macroscopic continuum models. As the *c.c.c.* is obtained by collecting all parameters of the DLVO-potential, the microscopic picture is condensed in this constant. On the other hand, within DLVO-theory bulk concentrations describe the concentration values outside the EDL regime. Thus, exactly these bulk concentrations can be interpreted as the macroscopic densities, which enter continuum mechanical models. Furthermore, from a microscopic point of view, bulk concentrations are given constants, whereas from a macroscopic point of view, bulk concentrations are variable densities. Thus, the connection between microscopic DLVO-theory and macroscopic continuum models is to identify the bulk concentration ρ_b of the negatively charged particles with the macroscopic concentration ρ^- . Thereby, we obtain from (3.7) the criterion for coagulation

$$\rho^- \geq c.c.c. \implies \begin{array}{l} \text{no microscopic energy barrier} \\ \text{according to DLVO-theory} \end{array} \implies \text{coagulation.}$$

Thus, we now define the barrier function g^{DLVO} from (3.4) by

$$g^{DLVO} = \rho^- - c.c.c. \quad (3.8)$$

Consequently, according to (3.2) and (3.5) we propose for coagulation the following stoichiometry



In conclusion, this leads us with (3.4), (3.6), and (3.8) to the coagulation rate function

$$R^{coag} = k^f H(\rho^- - c.c.c.) (y^+)^2.$$

4 Mathematical Model for Coagulation

First of all, we recall that the mixture density ρ is a given constant due to assumption (M6). Thus, we transform R^{coag} with $\rho^+ = \rho y^+$ to

$$R^{coag} = \underbrace{\rho^{-2} k^f}_{=: \tilde{k}^f} H(\rho^- - c.c.c.) (\rho^+)^2 = \tilde{k}^f H(\rho^- - c.c.c.) (\rho^+)^2.$$

¹Note that in [23] the formula for *c.c.c.* is slightly different, as *c.c.c.* is given in units [mol/L], whereas we convert *c.c.c.* to [kg/m³]

For ease of readability, we henceforth again write k^f instead of \tilde{k}^f . By substituting this equation and the additional preceding observations into the model equations from Section 2, we finally obtain the proposed continuum model for coagulation in electrolyte solutions:

1. Poisson's equation: We have for the electric field $\mathbf{E} = -\nabla\Phi$, and Φ solves

$$-\nabla \cdot (\epsilon_r \nabla \Phi) = \frac{1}{\epsilon_0} \rho_f \quad \text{with} \quad \rho_f = \sum_l \frac{e_0 z_l}{m_l} \rho_l = \frac{z\rho^+}{m^+} - \frac{z\rho^-}{m^-} + \frac{z\rho_a^+}{m^+}. \quad (4.1a)$$

2. Nernst–Planck equations: We have

$$\partial_t \rho^+ + \nabla \cdot \left(\rho^+ \mathbf{u} - d^+ \nabla \rho^+ - \frac{e_0 d^+ z}{k_b T} \rho^+ \mathbf{E} \right) = -2m^+ R^{coag}, \quad (4.1b)$$

$$\partial_t \rho^- + \nabla \cdot \left(\rho^- \mathbf{u} - d^- \nabla \rho^- + \frac{e_0 d^- z}{k_b T} \rho^- \mathbf{E} \right) = 0, \quad (4.1c)$$

$$\partial_t \rho_a^+ + \nabla \cdot \left(\rho_a^+ \mathbf{u} - d_a^+ \nabla \rho_a^+ - \frac{2e_0 d_a^+ z}{k_b T} \rho_a^+ \mathbf{E} + \frac{2d_a^+ m^+}{k_b T} \rho_a^+ \mathbf{g} \right) = 2m^+ R^{coag}. \quad (4.1d)$$

Here, the coagulation rate function R^{coag} is given by

$$R^{coag} = k^f H(\rho^- - c.c.c.) (\rho^+)^2, \quad (4.1e)$$

and the solvent concentration ρ_s is obtained by $\rho_s = \rho - \rho^+ - \rho^- - \rho_a^+$.

3. Navier–Stokes equations: For the barycentric momentum density holds

$$\nabla \cdot \mathbf{u} = 0, \quad (4.1f)$$

$$\rho \partial_t \mathbf{u} + \rho \nabla \cdot (\mathbf{u} \otimes \mathbf{u}) = -\nabla p + 2\eta \Delta \mathbf{u} + \rho_f \mathbf{E}. \quad (4.1g)$$

The mass production rates are subject to conservation of total mass and charges, cf. [11, 14, 45]. Furthermore, this model is a closed, as we have $5 + n$ equations (4.1a)–(4.1d), (4.1f), (4.1g) for the $5 + n$ unknowns

$$(\Phi, \rho^+, \rho^-, \rho_a^+, p, \mathbf{u}) \in \mathbb{R}^{5+n}.$$

Next, we note that in situations with vanishing barycentric flow, we apparently have $\mathbf{u} \equiv 0$. Substituting this into equations (4.1f) and (4.1g) shows that the Navier–Stokes equations reduce to $\nabla p = \rho_f \mathbf{E}$. Thus, in case of vanishing barycentric flow the pressure ∇p is determined up to a constant by Φ and the concentrations ρ^+ , ρ^- , and ρ_a^+ , as we have $\mathbf{E} = -\nabla\Phi$ and ρ_f defined in (4.1a). Consequently, in these situations the vector of primal unknowns is given by

$$(\Phi, \rho^+, \rho^-, \rho_a^+) \in \mathbb{R}^4,$$

and the model equations (4.1a)–(4.1g) reduce to

Poisson–Nernst–Planck system:

$$-\nabla \cdot (\epsilon_r \nabla \Phi) = \frac{1}{\epsilon_0} \rho_f \quad \text{with} \quad \rho_f = \sum_l \frac{e_0 z_l}{m_l} \rho_l = \frac{z\rho^+}{m^+} - \frac{z\rho^-}{m^-} + \frac{z\rho_a^+}{m^+}, \quad (4.2a)$$

$$\partial_t \rho^+ + \nabla \cdot \left(\rho^+ \mathbf{u} - d^+ \nabla \rho^+ - \frac{e_0 d^+ z}{k_b T} \rho^+ \mathbf{E} \right) = -2m^+ R^{coag}, \quad (4.2b)$$

$$\partial_t \rho^- + \nabla \cdot \left(\rho^- \mathbf{u} - d^- \nabla \rho^- + \frac{e_0 d^- z}{k_b T} \rho^- \mathbf{E} \right) = 0, \quad (4.2c)$$

$$\partial_t \rho_a^+ + \nabla \cdot \left(\rho_a^+ \mathbf{u} - d_a^+ \nabla \rho_a^+ - \frac{2e_0 d_a^+ z}{k_b T} \rho_a^+ \mathbf{E} + \frac{2d_a^+ m^+}{k_b T} \rho_a^+ \mathbf{g} \right) = 2m^+ R^{coag}. \quad (4.2d)$$

Here, the coagulation rate function $R^{coa g}$ is given by

$$R^{coa g} = k^f H(\rho^- - c.c.c.) (\rho^+)^2 . \quad (4.2e)$$

This subsystem of the model equations (4.1a)–(4.1g) still captures the interplay between coagulation, diffusion, and electric drift motion. More precisely, coagulation, diffusion, and electric drift motion are precisely the essential processes in almost all systems, in which coagulation occur. Thus, the restriction to $\mathbf{u} \equiv 0$ and to equations (4.2a)–(4.2e) still encompasses most of the relevant systems.

Finally, we numerically solve the model equations (4.2a)–(4.2e) in two space dimensions. Thereby, we demonstrate that this model is capable to produce the expected coagulation kinetics. Concerning the computational setup, we choose as time interval $I := [0, 60]$ and as spatial computational domain $\Omega \in \mathbb{R}^2$, the rectangle $\Omega := [0, 1] \times [0, 2]$. The boundary Γ of this domain, we split into the upper boundary Γ^a , the lower boundary Γ^b , the left boundary Γ^l , and the right boundary Γ^r , which are respectively defined by

$$\Gamma^a := [0, 1] \times \{2\}, \quad \Gamma^b := [0, 1] \times \{0\}, \quad \Gamma^l := \{0\} \times [0, 2], \quad \Gamma^r := \{1\} \times [0, 2].$$

To obtain a computable model, we equip the preceding system of equations with the following initial conditions

$$\rho^+(0, x) \equiv 1, \quad \rho^-(0, x) \equiv 0, \quad \rho_a^+(0, x) \equiv 0,$$

and boundary conditions

$$\begin{aligned} \Phi &= 0 \text{ on } (\Gamma^a \cup \Gamma^b) \times I \quad \text{and} \quad \Phi = c^{neg} < 0 \text{ on } (\Gamma^l \cup \Gamma^r) \times I, \\ \left(-d^+ \nabla \rho^+ - \frac{e_0 d^+ z}{k_b T} \rho^+ \mathbf{E} \right) \cdot \boldsymbol{\nu} &= 0 \text{ on } \Gamma \times I, \\ \left(-d^- \nabla \rho^- + \frac{e_0 d^- z}{k_b T} \rho^- \mathbf{E} \right) \cdot \boldsymbol{\nu} &= h^{in} \text{ on } \Gamma \times I, \\ \left(-d_a^+ \nabla \rho_a^+ - \frac{2e_0 d_a^+ z}{k_b T} \rho_a^+ \mathbf{E} + \frac{d_a^+ m_a^+}{k_b T} \rho_a^+ \mathbf{g} \right) \cdot \boldsymbol{\nu} &= 0 \text{ on } \Gamma \times I. \end{aligned}$$

In particular, the inflow function h^{in} is given by

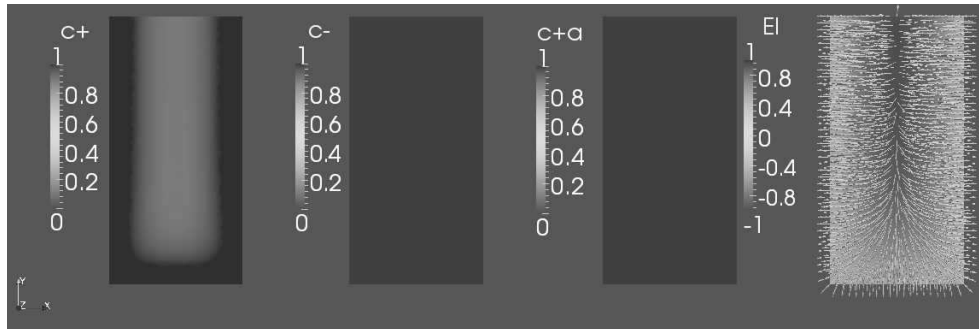
$$h^{in}(t, x) = \begin{cases} c^{in} \chi_{[5,10]}(t), & \text{on } \Gamma^a \times I, \\ 0, & \text{on } (\Gamma \setminus \Gamma^a) \times I. \end{cases}$$

Here, c^{in} is a given constant and $\chi_A(t)$ is the characteristic function for any set $A \in \mathbb{R}$, i.e.,

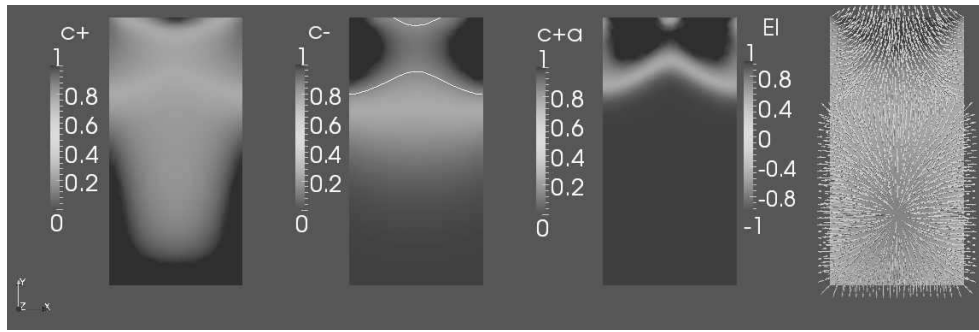
$$\chi_A(t) = \begin{cases} 1, & \text{if } t \in A, \\ 0, & \text{else.} \end{cases}$$

For the following simulation, we choose purely academic values for the coefficients. More precisely, we set $c^{neg} = 0.5$, $c^{in} = 0.2$, $d^+ = d^- = 0.1$, $d_a^+ = 0.01$, $z = 1$, $m^+ = 0.5$, $e_0/(k_b T) = 10$, $\epsilon_r = 0.1$, $e_0/\epsilon_0 = 0.8$, $k^f = 2.5$, $c.c.c. = 0.75$. Furthermore, as discretization parameters we use the time step size $\tau = 0.1$ and the mesh fineness $h = 0.05$, cf. [27, 31, 47]. This computational setup produces the following dynamics:

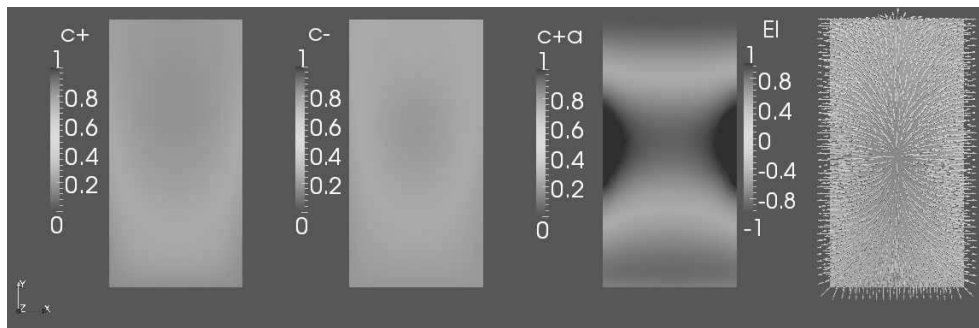
- (i) We can imagine Ω as a cross section of an idealized container, which is closed at the bottom, on the left, and on the right. Furthermore, this container possesses a constant surface potential c^{neg} on the left wall and right wall. This forces the positively charged particles to accumulate at Γ^l resp. Γ^r , see Figure 2. In this figure, the solutions of equations (4.2a)–(4.2e) are plotted as follows: From left to right, we have the concentration profiles of ρ^+ , ρ^- , ρ_a^+ , and the electric potential Φ together with the electric field lines.

Figure 2: Plot of the solutions at time $t = 0.8$

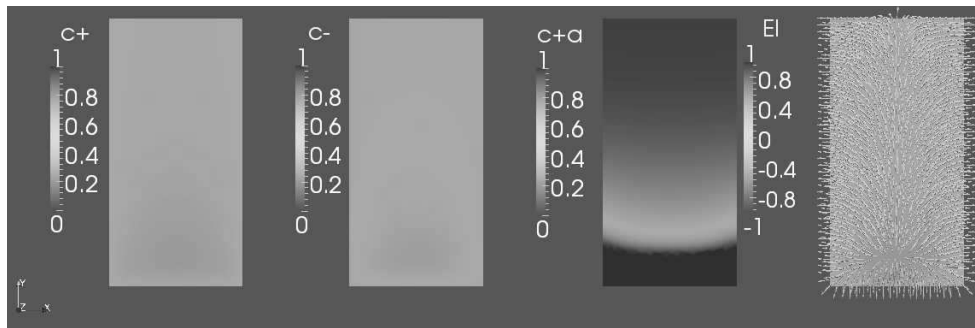
- (ii) Initially, the only solute present is ρ^+ , and in the time interval $[5, 10]$, we have an inflow of ρ^- from above. According to (4.2e), this causes ρ^+ to coagulate, if we have $\rho^-(t_0, x_0) > c.c.c.$, cf. Figure 3. Here, the ordering of the solutions is identical to Figure 2, and *c.c.c.* is depicted by the white contour line in the second picture.

Figure 3: Plot of the solutions at time $t = 8.9$

- (iii) The inflow of ρ^- stops at $t = 10$. However, due to gravitational forces the aggregates continue to settle, cf. Figure 4. Again, the solutions are ordered as in Figure 2.

Figure 4: Plot of the solutions at time $t = 25.6$

- (iv) Finally, the dynamics come to standstill with the aggregates accumulated at the bottom, cf. Figure 5. The solutions are again in the ordering of Figure 2.

Figure 5: Plot of the solutions at time $t = 60$

This numerical simulation was carried out in the software HyPHM, cf. [16], which is a finite element library based on MATLAB, cf. [38]. More precisely, we applied Gummel-iteration, cf. [19], to linearize the nonlinear system (4.1a)–(4.1g). The resulting sequence of linearized systems, we discretized by Raviart-Thomas element of lowest order in space and by the implicit Euler scheme in time, cf. [5, 47, 49]. For further details to numerical investigations of Poisson–Nernst–Planck systems, we refer, e.g., to [9, 17, 18, 20, 22, 50].

5 Conclusion

In this paper we presented a model for coagulation in electrolyte solutions. In Section 2, we started with the well-known Navier–Stokes–Poisson–Nernst–Planck system as model for electrolyte solutions. We chose this model for electrolyte solutions, since it is a thermodynamical consistent continuum model, which captures the coupled interplay of long-range electrostatic interaction, hydrodynamics, and mass transport. Moreover, we used this continuum model, as continuum models naturally account for many-body effects, which are important for a better understanding of coagulation. In this paper, we proposed to include coagulation phenomena in the Navier–Stokes–Poisson–Nernst–Planck system by modeling coagulation in terms of a reaction rate R^{coag} . For this coagulation rate R^{coag} , we derived formula (4.1e) in Section 3. This formula included both, the energetic picture of coagulation according to DLVO-theory, and the kinetic picture of coagulation in terms of the stoichiometry (3.5). Secondly, by means of (4.1e), we connected the atomistic DLVO-theory with the continuum Navier–Stokes–Poisson–Nernst–Planck system. Thereby, we combined two classical theories for electrolyte solutions, which actually have been developed on different spatial scales. In Section 4, this finally resulted in the model (4.1a)–(4.1g), which contained the microscopic picture condensed in the critical coagulation concentration (*c.c.c.*). Moreover, we demonstrated that the presented model for coagulation even captures most of the relevant systems, if we confine ourselves to situations with vanishing barycentric flow. Finally, in this case we presented numerical computations, which showed that the resulting model is capable to produce the expected dynamics of coagulation in electrolyte solutions. In conclusion, this paper presented a first step towards the modeling of coagulation in electrolyte solutions based on micro-macro continuum models.

Finally, we note that there are two generalizations of the presented model and the presented computations. Firstly, to clearly distinguish between the dissolved particles and the aggregates, we could reformulate the above model as multiphase model in the sense that we treat the aggregates as solid phase, whereas the fluid phase consists of the solvent and the solutes. Such a two-phase approach renders the illustrative but limited interpretation of ρ^+ and ρ_a^+ as size classes superfluous. Secondly, the numerical computations can be extended to multiscale numerics in the sense that the critical coagulation concentration (*c.c.c.*) can be locally computed at each degree of freedom by solving suitable microscopic problems. This would fully reveal the micro-macro character of the presented model. Both of these generalizations are currently under preparation and will be presented in forthcoming articles.

Acknowledgements

M. Herz was supported by the Elite Network of Bavaria.

References

- [1] J. S. Abel et al. "Sedimentation in flocculating colloidal suspensions." In: *Journal of Materials Research* 9.2 (1994), pp. 45–461.
- [2] H. Amann. "Coagulation-fragmentation processes." In: *Archive for Rational Mechanics and Analysis* 151.4 (2000), pp. 339–366.
- [3] P. Atkins and J. de Paula. *Physical Chemistry*. Freeman, 2006.
- [4] D. Bothe and W. Dreyer. "Continuum thermodynamics of chemically reacting fluid mixtures." WIAS preprint no 1909 (2013).
- [5] F. Brezzi and M. Fortin. *Mixed and hybrid finite elements methods*. Springer, 1991.
- [6] S. Buhmann and D.-G. Welsch. "Dispersion forces in macroscopic quantum electrodynamics." In: *Progress in Quantum Electronics* 31.2 (2007), pp. 51–130.
- [7] M. Burger, V. Capasso, and D. Morale. "On an Aggregation Model with Long and Short Range Interactions." In: *Nonlinear Analysis: Real World Applications* 8.3 (2007), pp. 939–958.
- [8] K. Chen and M. Elimelech. "Aggregation and deposition kinetics of fullerene (C60) nanoparticles." In: *Langmuir* 22.26 (2006), pp. 10994–11001.
- [9] Z. Chen and B. Cockburn. "Error estimates for a finite element method for the drift-diffusion semiconductor device equations." In: *SIAM Journal on Numerical Analysis* 31.4 (1994), pp. 1062–1089.
- [10] B. Davies and B. Ninham. "Van der Waals forces in electrolytes." In: *The Journal of Chemical Physics* 56.12 (1972), pp. 5797–5801.
- [11] S. De Groot and P. Mazur. *Non-Equilibrium Thermodynamics*. North-Holland Publishing, 1969.
- [12] J. K. G. Dhont. *An Introduction to Dynamics of Colloids*. Elsevier, 1996.
- [13] *DLV03.svg*. Accessed: 12 June 2013. Downloaded from Wikimedia Commons, the free media repository. URL: <http://commons.wikimedia.org/wiki/File:DLV03.svg>.
- [14] C. Eck, H. Garcke, and P. Knabner. *Mathematische Modellierung*. 2nd ed. Springer, 2011.
- [15] M. Elimelech et al. *Particle Deposition and Aggregation, Measurement, Modeling and Simulation*. Butterworth-Heinemann, 1995.
- [16] F. Frank. *HyPHM*. Accessed: Feb. 25 2014. Chair of Applied Mathematics 1, University of Erlangen–Nuremberg. URL: <http://www1.am.uni-erlangen.de/HyPHM>.
- [17] F. Frank, N. Ray, and P. Knabner. "Numerical investigation of homogenized Stokes–Nernst–Planck–Poisson systems." In: *Computing and Visualization in Science* 14.8 (2011), pp. 385–400.
- [18] J. Fuhrmann. "Comparison and numerical treatment of generalized Nernst–Planck Models." WIAS preprint no 1940 (2014).
- [19] H. K. Gummel. "A self-consistent iterative scheme for one-dimensional steady state transistor calculations." In: *IEEE Transactions on Electron Devices* 11 (1964), pp. 455–465.
- [20] R. Hiptmair, R. Hoppe, and B. Wohlmuth. "Coupling problems in microelectronic device simulation." In: *Notes on Numerical Fluid Mechanics*. Ed. by W. Hackbusch and G. Wittum. Vol. 51. Vieweg, 1995, pp. 86–95.
- [21] M. Hounslow, R. Ryall, and V. Marshall. "Discretized population balance for nucleation, growth, and aggregation." In: *AIChE Journal* 34.11 (1988), pp. 1821–1832.

- [22] R. Hünlich et al. "Modelling and Simulation of Power Devices for High-Voltage Integrated Circuits." In: *Mathematics – Key Technology for the Future*. Ed. by W. Jäger and H.-J. Krebs. Springer, 2003, pp. 401–412.
- [23] R. J. Hunter. *Foundations of Colloid Science*. 2nd ed. Oxford University Press, 2007.
- [24] A. Islam, B. Chowdhry, and M. Snowden. "Heteroaggregation in colloidal dispersions." In: *Advances in Colloid and Interface Science* 62.2-3 (1995), pp. 109–136.
- [25] J. N. Israelachvili. *Intermolecular and Surface Forces*. 3rd ed. Academic Press, 2011.
- [26] M. Kahlweit. "Kinetics of formation of association colloids." In: *Journal of Colloid And Interface Science* 90.1 (1982), pp. 92–99.
- [27] P. Knabner and L. Angermann. *Numerical Methods for Elliptic and Parabolic Partial Differential Equations*. Vol. 44. Texts in Applied Mathematics. New York: Springer, 2003.
- [28] P. Knabner, C. van Duijn, and S. Hengst. "An analysis of crystal dissolution fronts in flows through porous media. Part 1: Compatible boundary conditions." In: *Advances in Water Resources* 18.3 (1995), pp. 17–185.
- [29] M. Kobayashi et al. "Aggregation and charging of colloidal silica particles: Effect of particle size." In: *Langmuir* 21.13 (2005), pp. 5761–5769.
- [30] L. Landau and E. Lifshitz. *Statistical Physics, Part 2*. Vol. 9. Course of Theoretical Physics. Butterworth-Heinemann, 1980.
- [31] M. G. Larson and F. Bengzon. *The Finite Element Method: Theory, Impelemtation, and Practice*. Springer, 2010.
- [32] M. Lattuada, H. Wu, and M. Morbidelli. "A simple model for the structure of fractal aggregates." In: *Journal of Colloid and Interface Science* 268.1 (2003), pp. 106–120.
- [33] M. Lattuada et al. "Aggregation kinetics of polymer colloids in reaction limited regime: Experiments and simulations." In: *Advances in Colloid and Interface Science* 103.1 (2003), pp. 33–56.
- [34] J. Lyklema. *Fundamentals of Interface and Colloid Science*. Vol. IV: Particulate Colloids. Academic Press, 1995.
- [35] J. Lyklema, H. Van Leeuwen, and M. Minor. "DLVO-theory, a dynamic re-interpretation." In: *Advances in Colloid and Interface Science* 83.1 (1999), pp. 33–69.
- [36] A. J. Madja and A. L. Bertozzi. *Vorticity and Incompressible Flow*. Cambridge University Press, 2002.
- [37] J. H. H. Masliyah and S. Bhattacharjee. *Electrokinetic and Colloid Transport Phenomena*. Wiley Interscience, 2006.
- [38] MATLAB. *Release 2012b*. Natick, Massachusetts: The MathWorks Inc., 2012.
- [39] D. Morale, V. Capasso, and K. Oelschläger. "An interacting particle system modelling aggregation behavior: from individuals to populations." In: *Journal of Mathematical Biology* 50.1 (2005), pp. 49–66.
- [40] B. W. Ninham and P. Lo Nostro. *Molecular forces and self assembly*. Cambridge University Press, 2010.
- [41] B. Ninham. "On progress in forces since the DLVO theory." In: *Advances in Colloid and Interface Science* 83.1 (1999), pp. 1–17.
- [42] J. T. Oden. *An Introduction to Mathematical Modeling - A Course in Mechanics*. Wiley, 2011.
- [43] A. V. Parsegian. *Van Der Waals Forces*. Cambridge University Press, 2006.
- [44] Z. Peng, E. Doroodchi, and G. Evans. "DEM simulation of aggregation of suspended nanoparticles." In: *Powder Technology* 204.1 (2010), pp. 91–102.
- [45] I. Prigogine and D. Kondepudi. *Modern Thermodynamics*. Wiley, 1998.

- [46] R. F. Probstein. *Physiochemical Hydrodynamics – An Introduction*. 2nd ed. Wiley-Interscience, 2003.
- [47] A. Quarteroni and A. Valli. *Numerical Approximation of Partial Differential Equations*. Springer, 1994.
- [48] D. Ramkrishna. “Status of Population Balances.” In: *Reviews in Chemical Engineering* 3.1 (1985), pp. 49–95.
- [49] P. Raviart and J. Thomas. “A mixed finite element method for second-order elliptic problems.” In: *Mathematical Aspects of the Finite Element Method, Lectures Notes in Mathematics* 606 (1977), pp. 292–315.
- [50] N. Ray et al. “Multiscale Modeling of Colloid and Fluid Dynamics in Porous Media Including an Evolving Microstructure.” In: *Transport in Porous Media* 95.3 (2012), pp. 669–696.
- [51] W. Russel, D. Saville, and W. Schowalter. *Colloidal Dispersion*. Cambridge University Press, 1989.
- [52] R. Sanders, R. Chow, and J. Masliyah. “Deposition of Bitumen and Asphaltene-Stabilized Emulsions in an Impinging Jet Cell.” In: *Journal of Colloid And Interface Science* 174.1 (1995), pp. 230–245.
- [53] W. R. Smith and R. W. Missen. *Chemical reaction equilibrium analysis: theory and algorithms*. Wiley, 1982.
- [54] V. Smorodin. “Coagulation of charged nanoparticles: Refined classical approach and its limits.” In: 2008.
- [55] S. K. Upadhyay. *Chemical Kinetics and Reaction Dynamics*. Springer, 2007.
- [56] N. Van Kampen, B. Nijboer, and K. Schram. “On the Macroscopic Theory of Van der Waals Forces.” In: *Physics Letters* 26A.7 (1968), pp. 307–308.